TISSUE ENGINEERING: Part C
Volume 18, Number 1, 2012

DOI: 10.1089/ten.tec.2011.0060

Biofabrication of Osteochondral Tissue Equivalents by Printing Topologically Defined, Cell-Laden Hydrogel Scaffolds

Natalja E. Fedorovich, M.D., M.Sc.,[1,*] Wouter Schuurman, M.D.,[1,2,*] Hans M. Wijnberg, M.Sc.,[1] Henk-Jan Prins, M.Sc.,[3] P. René van Weeren, Ph.D.,[2] Jos Malda, Ph.D.,[1,4] Jacqueline Alblas, Ph.D.,[1] and Wouter J.A. Dhert, M.D., Ph.D.[1,5]

Osteochondral defects are prone to induce osteoarthritic degenerative changes. Many tissue-engineering approaches that aim to generate osteochondral implants suffer from poor tissue formation and compromised integration. This illustrates the need for further improvement of heterogeneous tissue constructs. Engineering of these structures is expected to profit from strategies addressing the complexity of tissue organization and the simultaneous use of multiple cell types. Moreover, this enables the investigation of the effects of three-dimensional (3D) organization and architecture on tissue function. In the present study, we characterize the use of a 3D fiber deposition (3DF) technique for the fabrication of cell-laden, heterogeneous hydrogel constructs for potential use as osteochondral grafts. Changing fiber spacing or angle of fiber deposition yielded scaffolds of varying porosity and elastic modulus. We encapsulated and printed fluorescently labeled human chondrocytes and osteogenic progenitors in alginate hydrogel yielding scaffolds of 1×2 cm with different parts for both cell types. Cell viability remained high throughout the printing process, and cells remained in their compartment of the printed scaffold for the whole culture period. Moreover, distinctive tissue formation was observed, both *in vitro* after 3 weeks and *in vivo* (6 weeks subcutaneously in immunodeficient mice), at different locations within one construct. These results demonstrate the possibility of manufacturing viable centimeter-scaled structured tissues by the 3DF technique, which could potentially be used for the repair of osteochondral defects.

Introduction

Osteochondral defects, affecting both articular cartilage and the underlying subchondral bone, are prone to induce osteoarthritic degenerative changes over time.[1] Current strategies to restore the biological and mechanical functionality of the joint include microfracture and mosaicplasty (autologous osteochondral grafting),[2–5] but their clinical use suffers from several limitations, including compromised cartilage tissue formation and donor site morbidity.[6] Further, in mosaicplasty it is difficult to match the shape of the injured site.[6] Current approaches for the engineering of osteochondral grafts suffer from poor tissue formation and compromised integration at the interface between the cartilage and bone layers[7–9] and between osteochondral graft and host tissue,[10] advocating the need for further improvement of these techniques.

An important focus in current cell-based tissue engineering lies on the development of engineered osteochondral tissues with design strategies that closely mimic the complex structure of matrix, cells, and bioactive factors assorted in a distinct spatiotemporal order inside native tissue.[11–13] Engineered (osteochondral) tissues can profit from the synergistic effects of combined growth factor delivery and heterotypic cell interactions on extracellular matrix (ECM) formation both *in vitro* and *in vivo*.[14–16] This biomimicking approach is expected to enhance graft functionality, render suitable mechanical properties to the engineered tissue,[17,18] and enhance the regenerative process. This was previously illustrated by the use of bilayered (hydrogel) scaffolds laden with multipotent stromal cells (MSCs) and chondrocytes, which supports the integration between the two layers.[14–16,19,20] For a further review of the literature on osteochondral implants, see Martin *et al.*[6] and O'Shea and Miao.[21]

[1]Department of Orthopaedics, University Medical Center Utrecht, Utrecht, The Netherlands.
[2]Department of Equine Sciences, Faculty of Veterinary Medicine, Utrecht University, Utrecht, The Netherlands.
[3]Department of Immunology, University Medical Center Utrecht, Utrecht, The Netherlands.
[4]Institute of Health and Biomedical Innovation, Queensland University of Technology, Brisbane, Australia.
[5]Faculty of Veterinary Medicine, Utrecht University, Utrecht, The Netherlands.
*These authors contributed equally to this work.

Organ or tissue printing by 3D fiber deposition (3DF) is an innovative approach in regenerative medicine, based on layered deposition of cell-laden hydrogel strands, and is derived from rapid-prototyping (RP) technology. With RP, 3D scaffolds with highly reproducible architecture (size, shape, porosity, interconnectivity, pore geometry, and orientation) and compositional variation can be created.[22] The porosity of the implants is easily tailored, which is important for mechanical and cell/tissue conductive properties. Interconnected porosity is of particular importance, as it facilitates nutrient supply and waste product removal[23] and allows ingrowth of blood vessels.[24] Using 3DF, living cells can be incorporated into the printed construct, creating grafts that further recapitulate the intricate 3D structure of cells and matrix in natural tissues.[25]

The aim of the present study is to build and characterize 3D structures for application in osteochondral tissue engineering and to validate organized cell placement inside printed grafts *in vitro* and *in vivo*. By combining human chondrocytes and human osteogenic progenitors with alginate hydrogel—a widely used polysaccharide that supports both chondrogenic and osteogenic differentiation,[26] we printed porous, heterogeneous constructs. We tested the design of various heterogeneous scaffolds and tailored the porosity and elastic modulus of grafts by modulating the distance between the strands and their configuration. The ensuing hybrid grafts were characterized for cell performance *in vitro* and for tissue development *in vivo*.

Materials and Methods

Hydrogel preparation and viscosity measurements

High-viscosity alginate powder (International Specialty Products [ISP]) was autoclaved and subsequently mixed (10%, w/v) overnight at 37°C either with MSC expansion medium (αMEM [Invitrogen] supplemented with 10% fetal bovine serum [FBS; Lonza], 0.1 mM ascorbic acid 2-phosphate [AsAP; Sigma-Aldrich], 2 mM L-glutamine [Glutamax; Invitrogen], 100 U/mL penicillin [Invitrogen], and 100 μg/mL streptomycin [Invitrogen]), osteogenic differentiation medium (MSC expansion medium supplemented with 10^{-8} M dexamethasone [Sigma-Aldrich] and 10 mM β-glycerophosphate [Sigma-Aldrich]), or chondrogenic differentiation medium (DMEM [Invitrogen] supplemented with 0.2 mM AsAP [Sigma-Aldrich], 0.5% human serum albumin [SeraCare Life Sciences], 1% [v/v] insulin–transferrin–selenium mixture [ITS-X; Invitrogen], 100 U/mL penicillin, 100 μg/mL streptomycin, and 5 ng/mL TGF-β_2 [R&D Systems]). Alginate was crosslinked with 102 mM aqueous $CaCl_2$ solution supplemented with 10 mM HEPES (pH 7.4; Invitrogen) for 15 min.

To determine the viscosity of the 10% (w/v) alginate, rheology analysis was performed on an ARG2 1000N rheometer (TA Instruments) using a cone-plate geometry (steel, 40 mm diameter with an angle of 2°) at 4°C. Shear rates between 1/s and 1500/s were applied for 10 min.

3DF presets

The BioScaffolder pneumatic dispensing system (SYS+ ENG) was used for 3D printing of hydrogel scaffolds. The prototype of this system is described in more detail elsewhere.[25,27] Briefly, the BioScaffolder is a three-axis dispensing machine, which builds 3D constructs by coordinating the motion of a pneumatic syringe dispenser (Supplementary Fig. S1; Supplementary Data are available online at www.liebertonline.com/tec). The dispenser deposits extrudate consisting of hydrogel either or not supplemented with cells on a stationary platform. Models of the scaffolds are loaded via computer-aided design/computer-aided manufacturing (CAD/CAM) software and translated for layer-by-layer fiber deposition by the machine (Fig. 1).

Effect of nozzle diameter, deposition speed and pressure, and fiber orientation

The inner nozzle diameter, deposition speed, and pressure were varied between 210 and 1610 μm, 100 and 300 mm/min, and 0.1 and 0.2 MPa, respectively, to assess their influence on strand size. Ten-layer rectangular 3D scaffolds of 10×10 mm with spacing between fibers of 0.8–2.5 mm and a layer thickness of 100 μm were constructed and subsequently crosslinked in $CaCl_2$ solution as indicated.

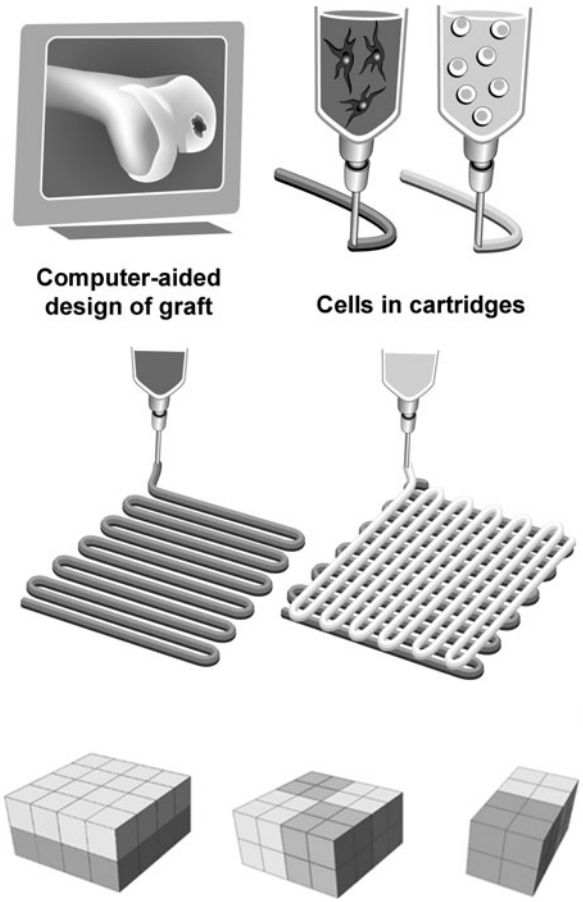

FIG. 1. Three-dimensional fiber deposition and characterization of the printing parameters. Schematic representation of tissue printing using various cell types; the design of a construct is translated to a robot arm that drives a cartridge loaded with a cell–hydrogel mixture and extrudes fibers in a layered fashion; the bottom panel represents various scaffold designs used in this study.

Fiber orientation was changed by plotting fibers with 45° or 90° angle steps between two successive layers (strand orientation (SO)45 and (SO)90, respectively). Flow rate of the hydrogel through a 210 μm inner nozzle diameter needle was determined for pressures of 0.15–0.6 MPa, by measuring the amount of extruded material per second (flow rate in mL/s). Shear stress was then determined according to the following formula: $(4Q/\pi\ r^3)\ \eta$, in which Q is flow rate (mm^3/s), r is radius of the needle (mm), and η is the viscosity (Pa·s).

Mechanical analysis of printed scaffolds of different porosity and SO

Alginate scaffolds of 7×7×0.8 mm (w×l×h) were prepared by varying the strand distance (SD) (0.8, 1.5, 2, and 2.5 mm at (SO)90, i.e., 90° relative to the underlying strand and (SO)90 and (SO)45 at 2 mm strand diameter). Subsequently, the scaffolds were crosslinked as described earlier.

Porosity was estimated by comparing the weight of the porous scaffolds to the weight of nonporous controls. The stiffness of the scaffolds was measured at room temperature using a dynamic mechanical analyzer (DMA 2980; TA Instruments) in controlled force mode. Scaffolds were placed between the parallel plates and a static force was applied between 0 and 1 N and varied at a rate of 0.1 N/min. The Young's modulus (E) was determined as previously described,[28] by measuring the variation of stress/strain ratio.

Deposition of acellular heterogeneous scaffolds

Heterogeneous scaffolds consisting of two different materials were designed, as illustrated in Figure 1. Alginate hydrogel was left translucent or stained with fast green, methylene blue, or basic fuchsin (pink) for illustration purposes and loaded into the BioScaffolder. Unless stated otherwise, an inner nozzle diameter of 420 μm was used, the speed of deposition was set at 300 mm/min, and the pneumatic pressure was set at 0.175 MPa to yield uniform, continuous extrusion of strands.

Cells

Human MSCs were isolated from bone marrow aspirates, obtained from donors undergoing hip arthroplasty after informed consent with approval of the local medical ethical committee, and culture expanded as previously described.[29] Briefly, aspirates were resuspended by using 20-gauge needles, plated at a density of 5×10^5 cells per square centimeter, and cultured in MSC expansion medium supplemented with 1 ng/mL recombinant human basic fibroblast growth factor (rhFGF2; 233-FB; R&D Systems). Medium was refreshed twice a week and cells were used for further subculturing. MSCs at passage 3–4 were used in these experiments.

Human articular chondrocytes (Chs) were isolated from cartilage, after informed consent with approval of the local medical ethical committee, from patients undergoing total knee arthroplasty. Cartilage was digested overnight using 0.15% collagenase type II (Worthington Biochemical) at 37°C. The cell suspension was filtered through a 100 mm cell strainer and washed in phosphate-buffered saline (PBS; Invitrogen). Cells were resuspended in chondrocyte expansion medium (DMEM [Invitrogen] supplemented with 10% FBS [Biowhittaker], 100 U/mL penicillin, 100 μg/mL streptomycin [Invitrogen], and 10 ng/mL rhFGF2 [R&D Systems]). Cells were then counted and seeded at a density of 5000 cells/cm^2 in expansion medium. For chondrocyte redifferentiation,[30] after 10 days the chondrocytes were detached using 0.25% trypsin (Invitrogen) and stored in liquid nitrogen until further use. Expanded chondrocytes were combined with alginate (2% [w/w] in differentiation medium)[31] at a density of 1×10^7 cells/mL. To create alginate beads, this solution was dripped with a 23G needle into 102 mM $CaCl_2$ solution supplemented with 10 mM HEPES (pH 7.4; Invitrogen). The beads were then cultured in chondrogenic differentiation medium for 5 days, and subsequently, cells were retrieved from the beads using sterile citrate buffer (150 mM sodium chloride and 55 mM sodium citrate [pH = 7.4]) for 15 min.

Viability analysis

To test the effect of shear stresses during the printing process on cell viability, hydrogel-embedded MSCs (5×10^6 cells/mL gel) were extruded through a needle with an inner nozzle diameter of 210 μm at various pressure settings (0.175–0.5 MPa). Unprinted cell-laden alginate was used as a control. The samples ($n = 5$ per group) were incubated in $CaCl_2$ solution and cultured for 5 or 24 h in expansion medium. The viability of the cells was determined by a LIVE/DEAD assay (Molecular Probes; MP03224) according to the manufacturer's recommendations. For this, five samples per condition were measured using a microscope equipped with an epifluorescence setup and excitation/emission setting of 488/530 nm to detect green fluorescence and 530/580 nm to detect red cells (Leica DM IRBE). Three randomly selected fields per sample were taken and cell viability was calculated as the average ratio of vital over total cells in a sample, determined from four randomly chosen fields per sample.

Fluorescent labeling and tracing of cells

Cells were fluorescently labeled for spatial distribution analysis. For this, Chs were incubated with PKH26 (20 μM, red; Sigma-Aldrich) and MSCs with CFSE (1 μM, green; Molecular Probes). The presence of fluorescent cells was directly analyzed after printing and after 14 and 21 days under a fluorescence microscope (Olympus BX51 microscope; Olympus DP70 camera) equipped with an epifluorescence setup and excitation/emission setting of 488/530 nm to detect green-fluorescent MSCs or 530/580 nm to detect red Chs (Leica DM IRBE).

Deposition of cell-laden scaffolds

To develop dual, heterogeneous scaffolds for *in vitro* use, fluorescently labeled MSCs and Chs were separately mixed with alginate at 5×10^6 and 3×10^6 cells/mL, respectively. A rectangular (1×2 cm), 10-layer scaffold was designed, which consisted of two parts (1×1 cm) directly adjacent to each other. The BioScaffolder interchanged the cooled cartridges (4°C) with the loaded syringes every two layers. The scaffolds were subsequently crosslinked in $CaCl_2$ solution.

For building heterogeneous scaffolds for *in vivo* implantation, an analogous protocol was followed: Chs (1×10^7 cells/mL) were mixed with alginate, and MSCs (1×10^7 cells/mL) were mixed with alginate supplemented with 10%

(w/v) osteoinductive biphasic calcium phosphate particles (BCPs; 80% ± 5% [w/v] hydroxyapatite and 20% ± 5% [w/v] β-tricalcium phosphate; total porosity 70% ± 5%, macroporosity 55% ± 5%, and microporosity 20% ± 5%). Irregularly shaped BCP particles (kindly provided by Progentix Orthobiology BV) were sintered at 1150°C and ranged from 106 to 212 μm in size. Acellular printed grafts served as negative controls. After printing, the constructs were cultured overnight and subcutaneously implanted in mice (see section "*In vivo* implantation").

Heterogeneous scaffold culture and embedding

Heterogeneous scaffolds were cultured in a 1:1 mixture of osteogenic and chondrogenic differentiation medium for a period of 7 and 21 days ($n = 4$ scaffolds for each time point). Scaffolds were maintained in a humidified incubator at 5% CO_2 and 37°C, and the medium was changed every 3 days. Additionally, the scaffolds were incubated for 15 min in 102 mM $CaCl_2$ once a week to prevent gel weakening (W. Schuurman, unpublished observation). Upon termination of the experiment, half of the experimental set of scaffolds was embedded in Tissue-Tek® (Sakura Finetek) and the others were dehydrated through graded ethanol series and embedded in paraffin. Samples were cut to yield 5 μm sections.

In vivo *implantation*

For *in vivo* assessment, printed Ch/MSC-laden grafts ($n = 6$) and acellular constructs consisting of an alginate part and an alginate/BCP part ($n = 4$) were cultured in proliferation medium for 24 h prior to implantation. Female nude mice (NMRI-Foxnu), 6 weeks old, were anaesthetized with 1.5% isoflurane, after which the implants were placed in separate subcutaneous dorsal pockets. The incisions were closed using a Vicryl 5-0 suture. The animals were postoperatively treated with the analgesic buprenorphine (0.05 mg/kg, sc; Temgesic) and housed in groups at the Central Laboratory Animal Institute, Utrecht University. Experiments were conducted with the permission of the local Ethical Committee for Animal Experimentation and in compliance with the Institutional Guidelines on the use of laboratory animals. After 6 weeks, the mice were killed and the constructs were harvested, fixed in 4% buffered formalin, decalcified in Luthra's solution (0.35 M HCl and 2.65 M formic acid in distilled water) for 24 h and processed for sections.

Analysis of differentiation of MSCs and Chs in vitro

Osteogenic differentiation of embedded cells was assessed by alkaline phosphatase (ALP) staining, collagen type I and osteonectin immunohistochemistry, and Alizarin red staining.

For the evaluation of ALP activity of encapsulated cells, cryosections were air-dried, fixed with 100% acetone for 10 min, and incubated in 0.2% (v/v) Triton X-100 in tris-buffered saline (TBS) for 10 min. The activity of ALP was determined by 30 min staining with the Fuchsin Substrate-Chromogen system (Dako). The presence of ALP-positive cells was analyzed with a light microscope and equipped with an Olympus DP70 camera. For immunocytochemical analysis, the paraffin sections were rehydrated and blocked in 0.3% (v/v) H_2O_2 in TBS for 10 min, followed by antigen retrieval in pronase (1 mg/mL; 10165921001; Roche Diagnostics) for 30 min at 37°C and hyaluronidase type II (10 mg/mL; H2126; Sigma-Aldrich) for 30 min at 37°C. The sections were then blocked in 5% (w/v) bovine serum albumin fraction V (BSA; Roche) in TBS for 30 min and incubated overnight at 4°C with either mouse anti-collagen type I antibody (2 μg/mL in 5% [w/v] BSA in TBS; clone I-8H5; Calbiochem) or mouse anti-osteonectin antibody (1/50 in 5% [w/v] BSA in TBS; clone AON-1; Developmental Studies Hybridoma Bank [DSHB]). A biotinylated secondary antibody was applied (1/200 in 5% [w/v] BSA in TBS; biotinylated sheep anti-mouse, RPN1001V1; GE Healthcare) for 1 h and the staining was enhanced by incubation with streptavidin–peroxidase for an additional hour (2 μg/mL; PN IM0309; Immunotec).

Chondrogenesis of encapsulated cells was assessed by safranin-O staining and collagen type II and VI immunohistochemistry. To demonstrate proteoglycan production, alginate was removed from the sections by 10 min incubation in citrate buffer and the sections were stained with Weigert's hematoxylin (Klinipath) and fast green (Merck) for cells and with Safranin-O (Merck) for proteoglycans. Immunohistochemical analysis of collagens was performed using a rabbit polyclonal antibody against collagen type II (10 μg/mL in 5% [w/v] BSA/PBS; Abcam 53047) and mouse anti-collagen type VI antibody (1/10 in 5% [w/v] BSA in TBS; clone 5C6; DSHB). Incubation with rabbit IgG or mouse isotype-matched control IgG (Dako) served as negative control for the staining. Subsequently, the secondary antibody was applied for 1 h: goat anti-rabbit Powervision (DPVR-55HRP; Immunologic) or goat anti-mouse HRP (10 μg/mL in 5% [w/v] BSA in TBS), respectively. All immunohistochemical stainings were developed with DAB and counterstained with Mayer's hematoxylin.

Analysis of printed tissue formed in vivo

Sections were stained with hematoxylin and eosin and Goldner's trichrome for general visualization of tissue development. To demonstrate formation of cartilaginous tissue, collagen types II and VI were immunolocalized, as indicated earlier.

To determine the presence of the osteogenic marker osteocalcin, immunohistochemical analysis was performed on rehydrated sections that were blocked in 5% (w/v) BSA in TBS for 30 min and incubated with rabbit polyclonal antibody to osteocalcin (2 μg/mL in 5% BSA/TBS; Alexis ALX-210-333; Enzo Life Sciences) overnight at 4°C. As secondary antibody, goat anti-rabbit HRP (1.6 μg/mL in 5% BSA/TBS; Dako) was applied for 1 h. For osteogenic marker collagen type I, immunohistochemical analysis was performed on rehydrated sections that were preincubated in 0.3% H_2O_2 for 10 min, followed by antigen retrieval with 10 mM sodium citrate buffer (pH 6.0) for 30 min at 95°C. The sections were then blocked in 5% (w/v) BSA in PBS for 30 min and incubated with rabbit polyclonal antibody to collagen type I (3.3 μg/mL in 5% BSA/PBS; Abcam 34710) overnight at 4°C. Incubation with rabbit IgG (Dako) served as negative control for the staining. As secondary antibody we used goat anti-rabbit HRP (2.5 μg/mL in 5% BSA/PBS; Dako) for 1 h. The staining was developed with DAB and counterstained with Mayer's hematoxylin.

Statistical analysis

Statistical analysis was performed with SPSS 12.0.1 software. A Mann–Whitney *U*-test was used to evaluate the viability data in printed and unprinted samples ($n=5$). This statistical test was chosen because of the small number of samples. A one-way analysis of variance with Bonferroni *post-hoc* test was used to analyze the viability data at different pressures and for the comparison of the Young's moduli of the different constructs. *p*-Values of less than 0.05 were considered statistically significant. Values are reported as mean ± standard deviation.

Results

3DF of structured hydrogel scaffolds

Defined, 3D hydrogel scaffolds consisting of up to 10 layers (0.8 mm) were printed by the BioScaffolder machine (Supplementary Fig. S1). Vertical pores were regular throughout the samples, whereas transversal pores fused because of the relative softness of the material. Strand size was tailored by adjusting the speed of deposition and the extrusion pressure (Fig. 2A–C). The shear-thinning effect that occurred in the system resulted in a fall in shear stress at higher extrusion pressures (Fig. 2D, E). The values calculated for the shear stress experienced by the (cell-laden) hydrogel inside the printer cartridge corresponded to those obtained using rheometer analysis (Fig. 2F).

Modulating the SD during printing resulted in formation of scaffolds with different porosities, and the resulting pore architecture of the printed scaffolds followed the imposed SO (Fig. 3A). To illustrate the effect of SO and SD on overall porosity and mechanical properties of the printed hydrogel scaffolds, SO and SD were varied between two successive layers. Increasing the SD from 0.8 mm to 1.5, 2.0, and 2.5 mm resulted in formation of scaffolds with 0, 35% ± 3%, 48% ± 7%, and 66% ± 4% porosity, respectively (Fig. 3A). Porosity in turn influences the elastic moduli of the scaffolds (Table 1). Increased scaffold porosities corresponded with a decrease in the elastic moduli of the scaffolds (Table 1). Changing SO relative to the underlying layer from (SO)90 to (SO)45 produced scaffolds with comparable porosity but higher elastic modulus (Table 1).

Heterogeneous scaffolds, consisting of two differently stained hydrogels, were printed according to the CAD/CAM design (Fig. 3B). The adjacent compartments, here indicated by different colors, interacted well without visible signs of delamination (Fig. 3B).

Printing of viable and heterogeneous cell-laden constructs

In the design of viable cell-laden structures, survival of the printed cells (Fig. 4A, B) is a crucial factor, and homogeneous cell dispersion allows uniform cell distribution throughout the construct. There were no statistically significant differences in cell survival at 5 h after printing (89% ± 2% viable cells in printed gels [$n=5$] vs. 89% ± 3% in unprinted controls [$n=5$]; $p=0.94$), indicating that the printing process did not induce immediate cell death in this system (Fig. 4C). We analyzed the effect of shear stress on the viability of printed MSCs, showing that 3DF printing sustains high viability of MSCs after 24 h in culture (viability of 88% ± 6% and 89% ± 7% in printed group [ø210 μm; 0.2 MPa] and unprinted

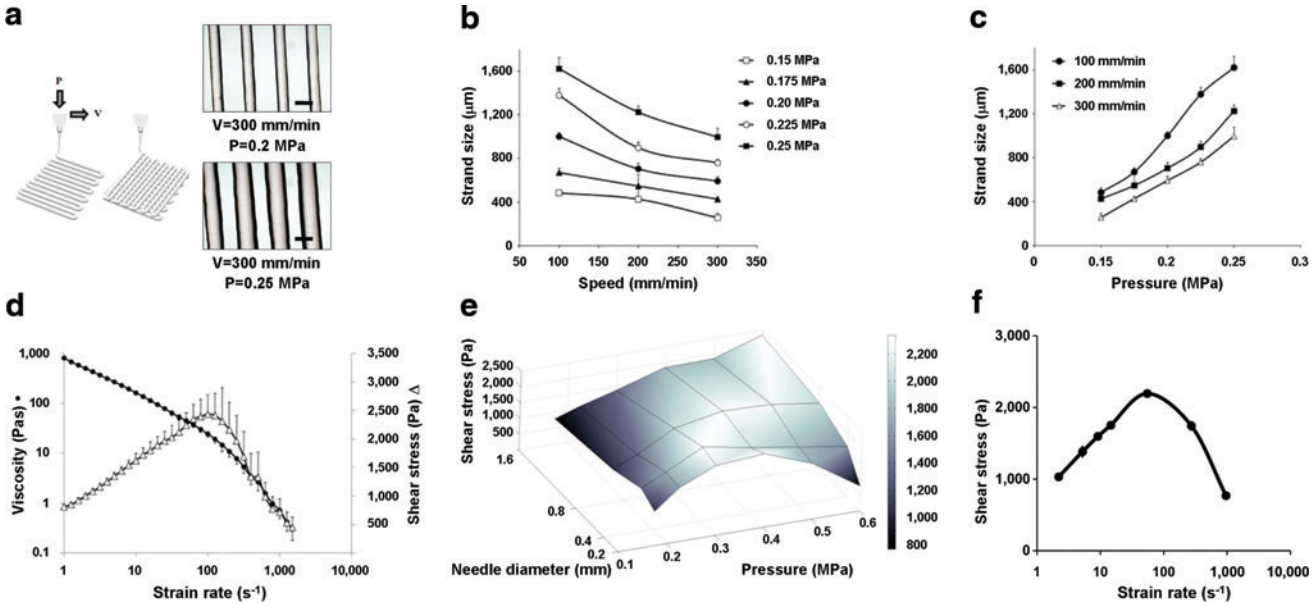

FIG. 2. The effect of printing parameters on strand size, strain rate, and shear stress. **(a)** The effect of speed of deposition (V) and pressure (P) on strand size. Scale bars: 500 μm. Strand size as function of speed **(b)** and pressure **(c)** shows that strand size is increased by decreasing printing speed or by increasing printing pressure. Data presented as mean ± standard deviation ($n=8$). **(d)** Viscosity (circles) and shear stress (triangles) of the hydrogel as a function of shear rate measured by rheometer ($n=6$). **(e)** Shear stress as a function of needle diameter and pressure ($n=4$), showing a shear-thinning effect at higher extrusion pressures, resulting in a fall in shear stress. **(f)** Shear stress in the BioScaffolder; calculated values for shear stress correspond to those obtained using rheometer analysis; values given as mean ± standard deviation ($n=4$). Color images available online at www.liebertonline.com/tec

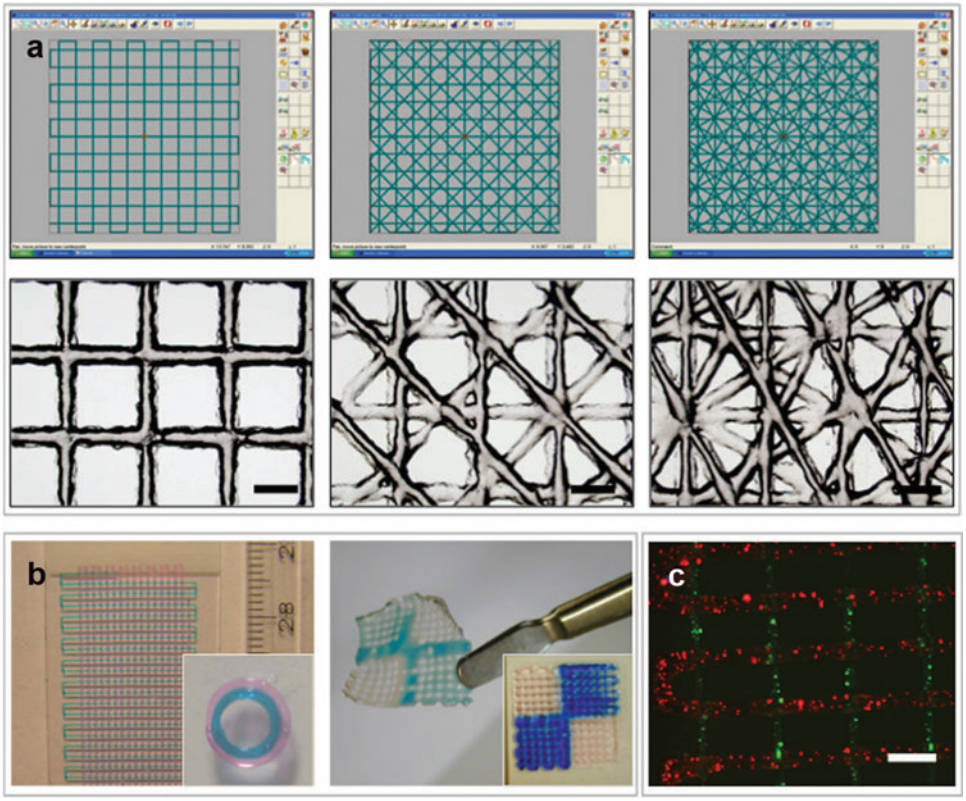

FIG. 3. Scaffold architecture. **(a)** A computer blueprint is used to construct scaffolds with variable strand orientation; computer-aided design/computer-aided manufacturing software design is shown in the top panels and light microscope images of resultant scaffolds in lower panels. Scale bar: 1 mm. Strand orientations of any layer in a design relative to the underlying layer from left to right is 90, 45, 30 (in degrees). **(b)** Examples of heterogeneous acellular scaffolds (left: multilayer and a circular construct with a diameter of 5 mm [inset]; right: a chess-board construct [blue dye is used for illustration purposes; no delamination between the printed alginate compartments]). **(c)** Encapsulated cells (fluorescently labeled red and green) in a heterogeneous scaffold, (SO)90. Scale bar: 1 mm. Color images available online at www.liebertonline.com/tec

control, respectively). Further, the viability of MSCs extruded at different pressures, and at different shear stresses, follows the inverse pattern of shear stress values (Fig. 4D).

An attractive feature of the 3DF approach is its ability to controllably place cells encapsulated in hydrogels and to combine different cell types. To illustrate the feasibility of printing cell-laden constructs with organizational diversity, different cell types were organized in layered configuration (Fig. 3C). Fluorescent detection of the cells demonstrates that the designed scaffold geometry is sustained by the entrapped cellular patterns *in vitro* (Fig. 6B).

Tissue formation by heterogeneous cell-laden constructs in vitro

To demonstrate the biological potential of 3DF using multiple cell types, we investigated cellular organization *in vitro*. Cell distribution differences in ECM formation were followed in time. For this, 10-layer alginate constructs were built, containing two adjacent regions with either MSCs or chondrocytes (Fig. 5A). Gross appearance of the implants indicated formation of two distinctive compartments starting 2 weeks after printing. The chondrocyte region exhibited thickening and increased opacity of the scaffold structure (Fig. 5A, lower panel), which was attributed to ECM deposition. In the MSC part, tissue formation was more subtle, as described later. The distribution of cell types was assessed for up to 3 weeks in culture by fluorescence labeling and showed strict containment of the printed population to either scaffold compartment, indicating good retention of organization *in vitro* (Fig. 6A, B). General histology of the composite scaffolds demonstrated appearance of cell clusters confined to the chondrocyte compartment, rich in cartilage-specific markers collagen VI and II (Figs. 5E and 6E). Concurrently in the osteogenic part, the cells remained homogeneously dispersed and stained positive for osteogenic markers ALP,

Table 1. Scaffold Strength as a Function of Porosity

	Solid	*Porous; (SO)90*	*Porous; (SO)90*	*Porous; (SO)90*	*Porous; (SO)45*
Porosity (%)	0	35 (3)	48 (7)	66 (4)	48 (2)
Modulus (kPa)	14.8 (3.6)	7.6 (0.6)[a,b]	5.6 (0.6)[a]	4.5 (0.1)[a]	6.4 (0.2)[a]
Strand distance	0.8 mm	1.5 mm	2.0 mm	2.5 mm	2.0 mm

Porosity (%), Young's modulus (kPa), and strand distance of the printed scaffolds (solid: $n=2$; porous: $n=4$) are given. Strand distance is the distance between the middle of two consecutive strands. A deposited strand distance of 0.8 mm yields solid constructs. (SO)90 and (SO)45 indicate a difference in SO relative to the underlying layer of 90° and 45°, respectively. Data are presented as mean ± standard deviation.

[a]Significantly different from solid construct ($p<0.05$).

[b]Significantly different ($p<0.05$) from construct (SO)90, with strand distance of 2.5 mm.

SO, strand orientation.

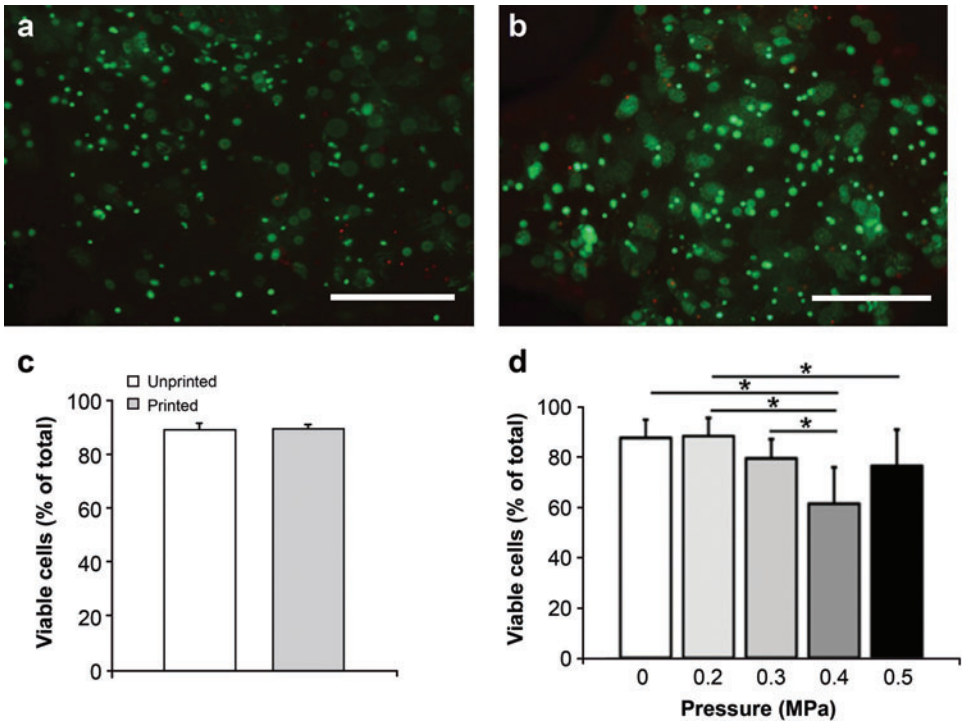

FIG. 4. The effect of printing process on MSC survival. **(a)** MSCs in unprinted control; red: dead cells, green: live cells. **(b)** MSCs in alginate at 5 h after printing. **(c)** Viability in unprinted (white) and printed (gray) samples ($n=5$) at 5 h after printing; the pneumatic pressure was set at 0.175 MPa. No significant differences between printed and unprinted samples were found ($p=0.94$). **(d)** Viability at 24 h after printing at various pressures ($n=4$). Controls (0 MPa) are nonprinted. *$p<0.05$. MSCs, multipotent stromal cells. Color images available online at www.liebertonline.com/tec

collagen type I, osteonectin, and Alizarin red (Figs. 5D and 6). Together these findings illustrate heterogeneous ECM formation *in vitro* analogous to the deposited cell type.

Tissue formation by heterogeneous cell-laden grafts in vivo

To validate the retention of heterogeneous tissue organization *in vivo*, we investigated the effect of 3DF-defined cell placement on osteochondral tissue formation in mice. Grafts were composed of a chondrocyte-laden compartment and an MSC-laden compartment, which included osteoinductive ceramic particles. Constructs exhibited heterogeneous tissue formation corresponding to the deposited cell type (Fig. 7) after 6 weeks. ECM formation was evidenced by Goldner's trichrome staining, and almost no matrix developed in acellular control gels (Fig. 7B, inset), signifying that embedded cells contribute substantially to formation of ECM in these grafts. Osteocalcin- (Fig. 7D) and collagen type I (not shown)-positive matrix enveloped the BCP particles, suggesting the onset of osteogenic differentiation in this part of the construct.

In the chondrocyte-laden region of the construct we observed dense matrix accumulations in alginate and formation

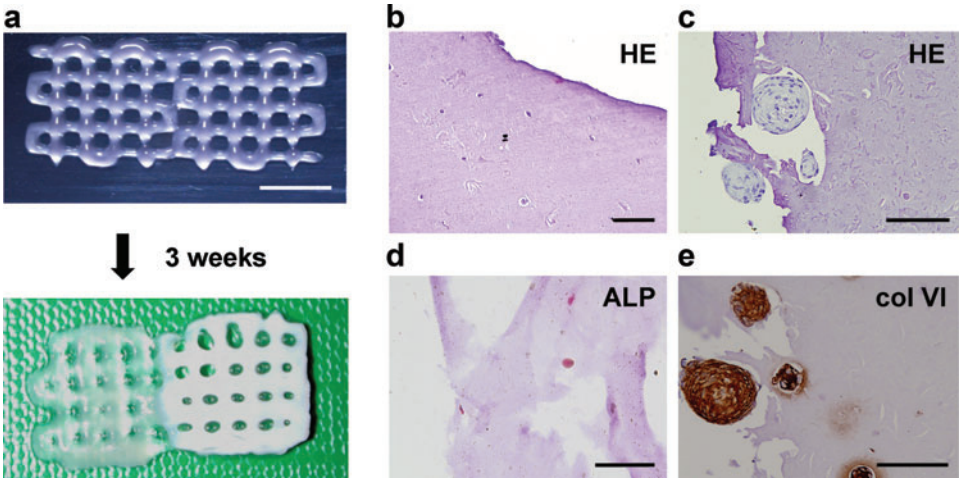

FIG. 5. Appearance and cell function in printed grafts *in vitro.* **(a)** Macroscopic appearance of printed composite constructs with an MSC-laden compartment on the left and a chondrocyte-laden compartment on the right, directly after printing (top) and after 3 weeks of culture (bottom), showing differences on a macroscopic level. Scale bar: 500 μm. HE staining after 21 days in osteogenic part **(b)** and chondrogenic part **(c)** illustrates clusters inside the alginate fiber in the chondrocyte part of the construct, whereas cells are dispersed in the MSC compartment. Cells: dark blue; alginate: light blue. **(d)** ALP staining (red) after 7 days demonstrates positive cells in MSC compartment of the construct. **(e)** Immunolocalization of collagen type VI (brown) at 21 days in the chondrocyte-laden part of the scaffold. Scale bars: 100 μm. HE, hematoxylin and eosin; ALP, alkaline phosphatase. Color images available online at www.liebertonline.com/tec

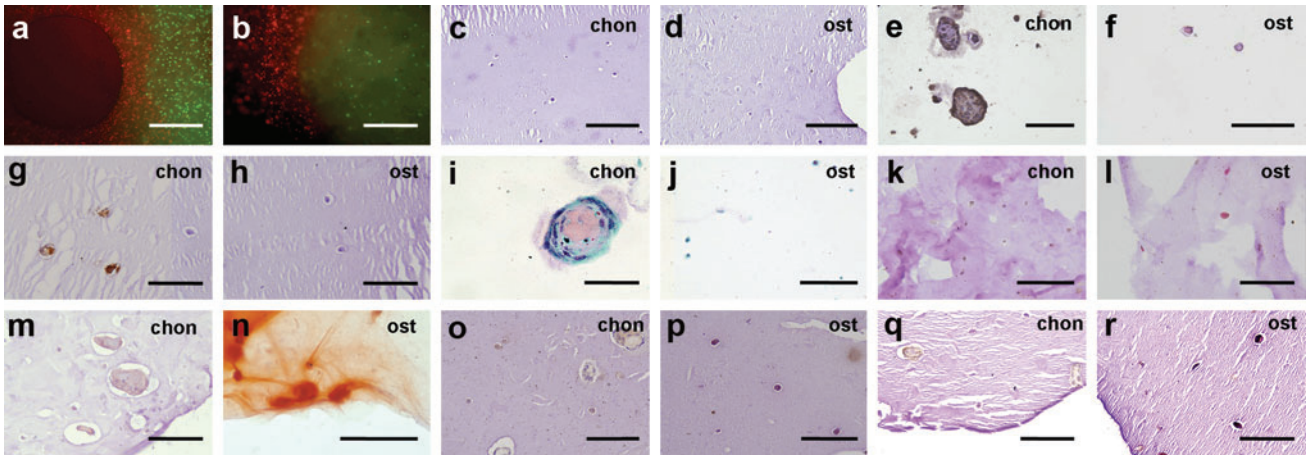

FIG. 6. Analysis of extracellular matrix formation in printed grafts *in vitro*. The MSC-laden osteogenic part is indicated with "ost" and the chondrocyte-laden part is indicated with "chon." **(a, b)** Fluorescently labeled cells (MSCs in green and chondrocytes in red) directly after printing **(a)** and after 3 weeks **(b)**. Scale bars: 500 μm. **(c, d)** HE staining after 7 days demonstrates homogeneous dispersion of cells in both regions of the scaffold, in chondrogenic part **(c)** and in osteogenic part **(d)**. Scale bars: 200 μm. **(e, f)** Immunolocalization of collagen type II (brown) after 21 days in chondrogenic part **(e)** and in osteogenic part **(f)**; the surrounding alginate has been washed away. Scale bars: 100 μm. **(g, h)** Immunolocalization of collagen type VI (brown) after 7 days, in chondrogenic part **(g)** and in osteogenic part **(h)**. Scale bars: 100 μm. **(i, j)** Safranin-O staining at 21 days indicates presence of proteoglycans (pink) in chondrocyte region **(i)**, and not in osteogenic part **(j)**; the surrounding alginate has been washed away. Scale bars: **(i)** 50 μm, **(j)** 100 μm. **(k, l)** ALP staining after 7 days demonstrates positive cells (red) in the osteogenic compartment of the construct **(l)** and not in chondrogenic part **(k)**. Scale bars: 100 μm. **(m, n)** Alizarin red staining for calcium depositions (orange-red) after 21 days in chondrogenic part **(m)** and in osteogenic part **(n)**. Scale bars: 100 μm. **(o, p)** Collagen type I immunostaining (brown) at 21 days in chondrogenic part **(o)** and in osteogenic part **(p)**. Scale bars: 100 μm. **(q, r)** Osteonectin immunostaining (brown) at 21 days in chondrogenic part **(q)** and in osteogenic part **(r)**. Scale bars: 100 μm. Color images available online at www.liebertonline.com/tec

of cell clusters positive for cartilage-specific markers collagen type II and VI (Figs. 7C and 8). The latter marker is specific for human collagen VI and does not cross-react with mouse tissue, indicating that the newly formed collagenous matrix is derived from the transplanted cells.

Discussion

In the present study, for the first time, the feasibility of 3DF to fabricate porous heterogeneous osteochondral constructs that encompass living chondrocytes and osteogenic progenitors is demonstrated. Printed cell-hydrogel constructs revealed differential lineage commitment and ECM formation. This study addresses recent development in the field of regenerative medicine that aims to recapitulate the complexity of natural biological tissues, consisting of different cell types with a specific organization and matrix composition.

Previously, 3DF was developed as an RP method to create 3D porous shapes of a range of materials, including thermoplastics[22,32] and hydrogels,[27] and the adapted technology used by us can comply with several important prerequisites of tissue-engineered grafts, including tailorable mechanical properties, the introduction of sufficient interconnected porosity, the introduction of living (progenitor) cells, and the possibility to investigate organizational aspects in tissue regeneration. Moreover, 3DF is a robust dispensing technology, resulting in constructs that easily reach relevant (cm-scale) sizes for tissue replacement. Addition of cells to the process of hydrogel fiber deposition facilitates formation of cell-laden, viable printed scaffolds for tissue engineering purposes,[25,33] and local cell densities can be modulated and various types of cells can be deposited in tissue-like architectures.

When adding cells to the materials before printing, we demonstrated that human primary stem cells survive the shear stresses imposed on them during the deposition process, which is in line with previous reports.[25,34] A relatively high cell survival was observed at higher dispensing pressures, which is explained by shear thinning of the hydrogel, resulting in a drop in shear stress. This phenomenon of shear thinning is a common behavior for (natural) polymers[35] and has been described in detail for minimal invasive material delivery.[36] As matrix stiffness is a known factor in cell differentiation,[37] modulating biomechanical properties by using various depositing configurations and materials is likely to influence tissue formation *in vitro* and *in vivo*.

The concurrent printing of different hydrogels illustrated the ability of the system to reproducibly print heterogeneous 3D structures comprising different matrices. The results show adequate integration between the adjacent layers of separately printed gels. As a following step we demonstrated the design of cell-laden heterogeneous scaffolds (i.e., printed with different cell types at different locations). In the heterogeneous grafts, *in vitro* studies revealed that the cells remained located specifically in their original deposited position during the entire culture period. This limited interaction between the cells of the adjacent layers can be explained by the hydrogel matrix employed for the encapsulation of the cells. Because of the noninteractive nature of alginate, the cells are unable to adhere or degrade the surrounding gel matrix[38] and will remain confined.

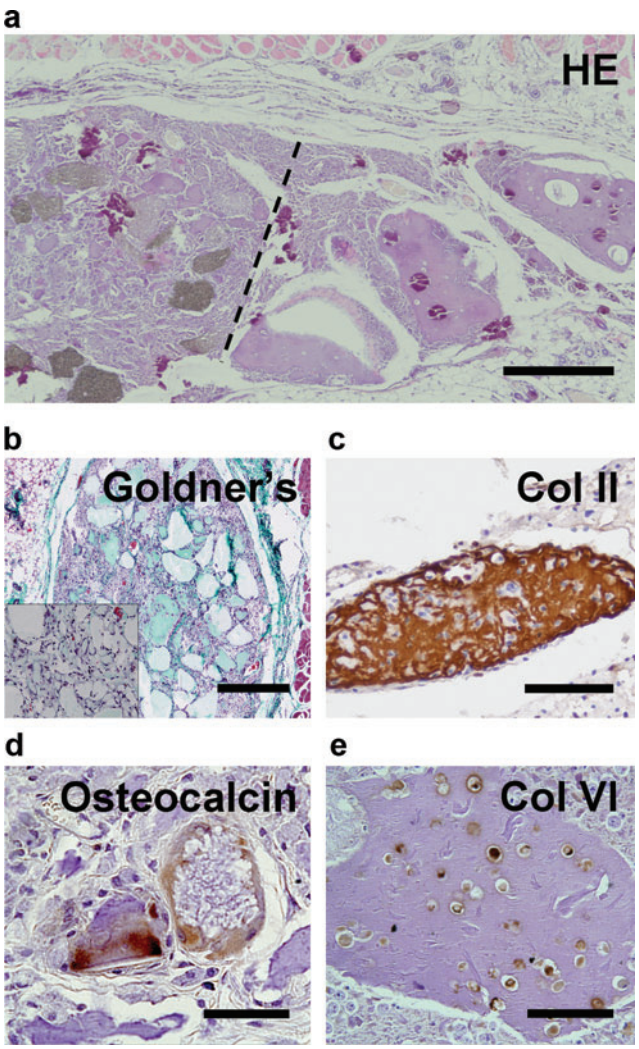

FIG. 7. Tissue development in printed scaffolds *in vivo*. **(a)** General histology (HE staining) of the graft illustrates heterogeneous tissue formation; alginate appears purple (dashed line represents the interface between MSC-laden region with biphasic calcium phosphate particles [gray, left] and Ch-laden alginate [right]). Scale bar: 500 μm. **(b)** Goldner's trichrome staining in MSC-laden part demonstrates ECM formation in the cell-laden grafts and limited tissue formation in acellular scaffolds (inset). Scale bar: 500 μm. **(c, e)** Immunostaining for cartilage-specific markers collagen types II **(c)** and VI **(e)** is positive in the chondrocyte-laden part of the grafts; alginate appears purple. Scale bars: 100 μm. **(d)** Immunostaining for osteocalcin (brown) demonstrates osteogenic differentiation in MSC-laden part of the grafts. Scale bar: 50 μm. Color images available online at www.liebertonline.com/tec

Our *in vivo* study demonstrated that in printed osteochondral grafts, specific structural arrangements imposed by 3DF may induce heterogeneous tissue formation and can lead to a stable cellular architecture, which is an important factor in the success of 3D constructs.[39] Another important characteristic for tissue engineering purposes is maintenance of the required phenotype.[40] Our printed osteochondral grafts exhibited heterogeneous ECM formation at defined locations within one scaffold, corresponding to the deposited cell type. The transplanted human cells contributed to ECM formation, as evidenced by detection of substantial amounts of human collagen matrix in the cellular grafts and absence of ECM in acellular gels. The lack of abundant osteogenic tissue formation in the osteochondral printed grafts may be explained by the use of low interactive alginate matrix with a relatively high polymer concentration. ECM formation deposition could be improved by optimizing preculture and perfusion regimes[41] or using hydrogels with lower viscosity combined with stiffer materials, which would also broaden the range of hydrogels that can be used.[42] The issue of vascularization of the bone grafts needs to be addressed in future studies in order to bring the scale-up of constructs to clinically relevant sizes within reach.

To design better cartilage implants, and larger bone grafts, design strategies should mimic anatomical and biochemical organization of cells, matrix, and growth factors found in the native tissue.[17,18,43] Various other cell-printing approaches, including 3D ink-jet printing[44] and 3D robotic dispensing,[34] have been previously applied for precise patterning of various cell populations. Similarly, micropatterning approaches, such as microfluidic patterning[45] and microcontact printing,[46] allow the study of cellular interactions between various populations and at different ratios. Each of these technologies copes with specific challenges, such as material choice, precision of the deposition, combining multiple components and cell types, stability of the construct, and depending on the application, the realization of relevant sized constructs. Although most of these technologies are very precise and reach high resolutions, the attained scale of the constructs is at maximum millimeter size. The 3DF technology presented in the present study is powerful in that respect, as centimeter-scale scaffolds are easily printed, making the technology an interesting option in tissue replacement therapies. Nevertheless, several important issues in 3DF still have to be addressed. First, the use of materials that possess the mechanical properties to enable printing and endure the forces acting on tissues, especially on cartilage and bone, and, at the same time, are biocompatible[47] should be considered. The materials so far used for 3DF result in variable cell viability and tissue responses,[48,49] the seemingly best performers being natural hydrogels. However, using model alginate gels in this study, only a limited height of the construct could be achieved. The limitations of alginate with respect to its low mechanical strength could be alleviated by the use of thermo- and photocurable hydrogels[50,51] or by the use of combination of hydrogels with biomaterials that possess higher mechanical strength.[42,52,53] Further modulations of mechanical properties of these hydrogel scaffolds with 3DF can potentially meet the mechanical requirements needed for tailored tissue engineering applications. Future advances in biomaterial sciences may provide more sophisticated and tailored materials that meet the 3DF requirements better. An additional challenge will be the *in vivo* implantation of heterogeneous printed grafts at orthotopic locations, at the same time maintaining the external shape and internal organization of the printed constructs and ensuring good integration with the surrounding host tissue. With respect to the biology of self-organization, organ printing with 3DF is a powerful tool to study the relevance of biomimicking, that is, to address the question whether

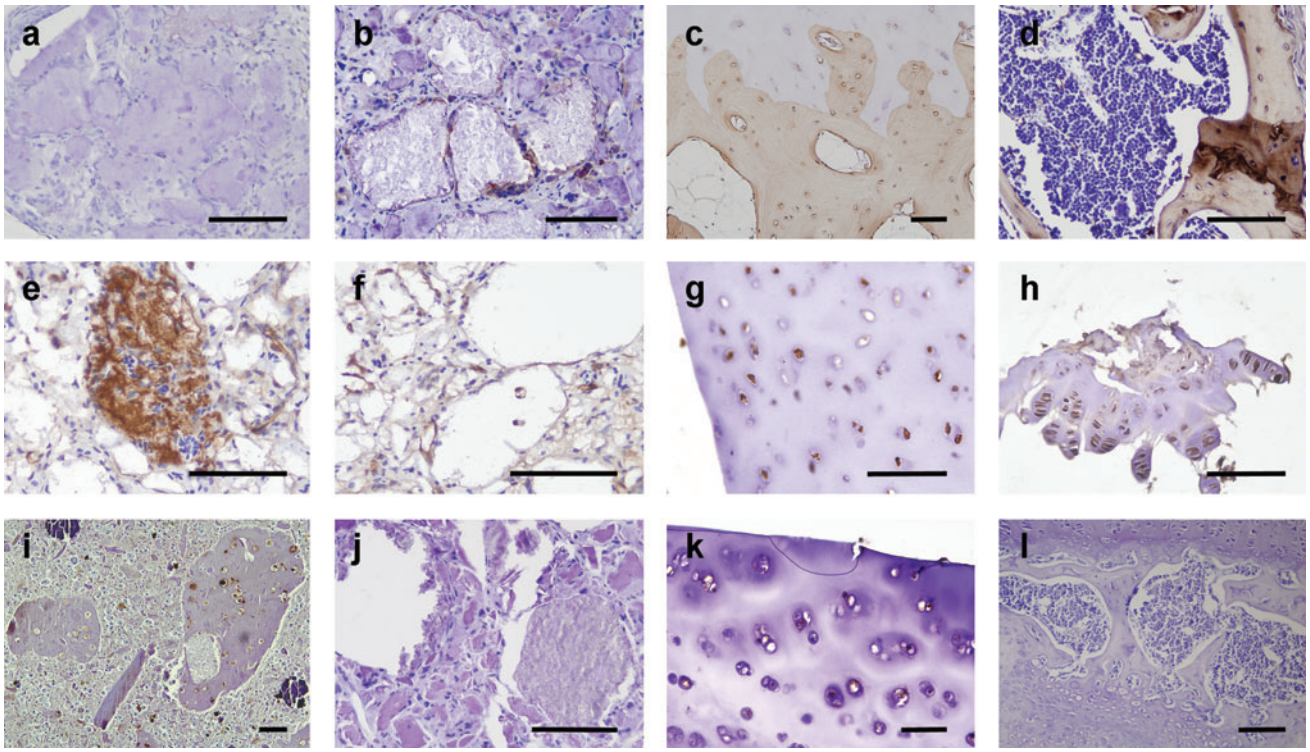

FIG. 8. Collagen production in printed scaffolds *in vivo*. **(a–d)** Collagen type I immunohistochemistry (brown) performed on explanted tissue after 6 weeks in chondrocyte-laden region **(a)**, MSC-laden region **(b)**, human osteochondral control tissue **(c)**, and a murine bone control **(d)**. **(e–h)** Collagen type II immunohistochemistry (brown) and **(i–l)** collagen type VI immunostaining (brown) on chondrocyte-laden region **(e, i)**, MSC-laden region **(f, j)**, human cartilage **(g, k)**, and murine cartilage **(h, l)**. Scale bars: 100 μm. Color images available online at www.liebertonline.com/tec

anatomical tissue design is an important prerequisite for the development of functional tissues.

Conclusions

In the present study, we demonstrate the possibility of manufacturing viable heterogeneous tissue constructs consisting of bone and cartilage matrix by a 3DF technique. We printed centimeter-scale intricate hydrogel scaffolds with high cell viability. By encapsulating osteogenic progenitors and chondrocytes in different parts of a construct, the formation of distinctive ECM regions *in vitro* and *in vivo* according to the anticipated tissue type was attained.

Acknowledgments

The collagen type VI antibody (developed by E. Engvall) and the osteonectin antibody (developed by J.D. Termine) were obtained from the DSHB. The authors thank Dr. T. Vermonden from the Department of Pharmaceutics, Utrecht University, for help with rheometry measurements. The authors acknowledge the financial support by the Anna Foundation, The Netherlands Organization for Scientific Research (NWO; grant no. 017.001.181), the Smart Mix Program of The Netherlands Ministry of Economic Affairs and The Netherlands Ministry of Education, Culture, and Science, and the Dutch Technology Foundation STW.

Disclosure Statement

No competing financial interests exist.

References

1. Prakash, D., and Learmonth, D. Natural progression of osteo-chondral defect in the femoral condyle. Knee **9,** 7, 2002.
2. Marcacci, M., Kon, E., Delcogliano, M., Filardo, G., Busacca, M., and Zaffagnini, S. Arthroscopic autologous osteochondral grafting for cartilage defects of the knee: prospective study results at a minimum 7-year follow-up. Am J Sports Med **35,** 2014, 2007.
3. Hangody, L., Vasarhelyi, G., Hangody, L.R., Sukosd, Z., Tibay, G., Bartha, L., and Bodo, G. Autologous osteochondral grafting—technique and long-term results. Injury **39 Suppl 1,** S32, 2008.
4. Kon, E., Gobbi, A., Filardo, G., Delcogliano, M., Zaffagnini, S., and Marcacci, M. Arthroscopic second-generation autologous chondrocyte implantation compared with microfracture for chondral lesions of the knee: prospective nonrandomized study at 5 years. Am J Sports Med **37,** 33, 2009.
5. Lane, J.G., Healey, R.M., Chen, A.C., Sah, R.L., and Amiel, D. Can osteochondral grafting be augmented with microfracture in an extended-size lesion of articular cartilage? Am J Sports Med **38,** 1316, 2010.
6. Martin, I., Miot, S., Barbero, A., Jakob, M., and Wendt, D. Osteochondral tissue engineering. J Biomech **40,** 750, 2007.
7. Schaefer, D., Martin, I., Shastri, P., Padera, R.F., Langer, R., Freed, L.E., and Vunjak-Novakovic, G. *In vitro* generation of osteochondral composites. Biomaterials **21,** 2599, 2000.
8. Gao, J., Dennis, J.E., Solchaga, L.A., Awadallah, A.S., Goldberg, V.M., and Caplan, A.I. Tissue-engineered fabrication of an osteochondral composite graft using rat bone marrow-derived mesenchymal stem cells. Tissue Eng **7,** 363, 2001.

9. Schaefer, D., Martin, I., Jundt, G., Seidel, J., Heberer, M., Grodzinsky, A., Bergin, I., Vunjak-Novakovic, G., and Freed, L.E. Tissue-engineered composites for the repair of large osteochondral defects. Arthritis Rheum **46,** 2524, 2002.
10. Theodoropoulos, J.S., De Croos, J.N., Park, S.S., Pilliar, R., and Kandel, R.A. Integration of tissue-engineered cartilage with host cartilage: an *in vitro* model. Clin Orthop Relat Res **469,** 2785, 2011.
11. Allan, K.S., Pilliar, R.M., Wang, J., Grynpas, M.D., and Kandel, R.A. Formation of biphasic constructs containing cartilage with a calcified zone interface. Tissue Eng **13,** 167, 2007.
12. Abrahamsson, C.K., Yang, F., Park, H., Brunger, J.M., Valonen, P.K., Langer, R., Welter, J.F., Caplan, A.I., Guilak, F., and Freed, L.E. Chondrogenesis and mineralization during *in vitro* culture of human mesenchymal stem cells on three-dimensional woven scaffolds. Tissue Eng Part A **16,** 3709, 2010.
13. Guo, X., Park, H., Young, S., Kretlow, J.D., van den Beucken, J.J., Baggett, L.S., Tabata, Y., Kasper, F.K., Mikos, A.G., and Jansen, J.A. Repair of osteochondral defects with biodegradable hydrogel composites encapsulating marrow mesenchymal stem cells in a rabbit model. Acta Biomater **6,** 39, 2010.
14. Alhadlaq, A., and Mao, J.J. Tissue-engineered osteochondral constructs in the shape of an articular condyle. J Bone Joint Surg Am **87,** 936, 2005.
15. Elisseeff, J., Puleo, C., Yang, F., and Sharma, B. Advances in skeletal tissue engineering with hydrogels. Orthod Craniofac Res **8,** 150, 2005.
16. Isogai, N., Landis, W., Kim, T.H., Gerstenfeld, L.C., Upton, J., and Vacanti, J.P. Formation of phalanges and small joints by tissue-engineering. J Bone Joint Surg Am **81,** 306, 1999.
17. Klein, T.J., Malda, J., Sah, R.L., and Hutmacher, D.W. Tissue engineering of articular cartilage with biomimetic zones. Tissue Eng Part B Rev **15,** 143, 2009.
18. Sharma, B., and Elisseeff, J.H. Engineering structurally organized cartilage and bone tissues. Ann Biomed Eng **32,** 148, 2004.
19. Alhadlaq, A., and Mao, J.J. Tissue-engineered neogenesis of human-shaped mandibular condyle from rat mesenchymal stem cells. J Dent Res **82,** 951, 2003.
20. Alhadlaq, A., Elisseeff, J.H., Hong, L., Williams, C.G., Caplan, A.I., Sharma, B., Kopher, R.A., Tomkoria, S., Lennon, D.P., Lopez, A., and Mao, J.J. Adult stem cell driven genesis of human-shaped articular condyle. Ann Biomed Eng **32,** 911, 2004.
21. O'Shea, T.M., and Miao, X. Bilayered scaffolds for osteochondral tissue engineering. Tissue Eng Part B Rev **14,** 447, 2008.
22. Woodfield, T.B., Malda, J., de Wijn, J., Peters, F., Riesle, J., and van Blitterswijk, C.A. Design of porous scaffolds for cartilage tissue engineering using a three-dimensional fiber-deposition technique. Biomaterials **25,** 4149, 2004.
23. Malda, J., Woodfield, T.B., van der Vloodt, F., Kooy, F.K., Martens, D.E., Tramper, J., van Blitterswijk, C.A., and Riesle, J. The effect of PEGT/PBT scaffold architecture on oxygen gradients in tissue engineered cartilaginous constructs. Biomaterials **25,** 5773, 2004.
24. Karageorgiou, V., and Kaplan, D. Porosity of 3D biomaterial scaffolds and osteogenesis. Biomaterials **26,** 5474, 2005.
25. Fedorovich, N.E., De Wijn, J.R., Verbout, A.J., Alblas, J., and Dhert, W.J. Three-dimensional fiber deposition of cell-laden, viable, patterned constructs for bone tissue printing. Tissue Eng Part A **14,** 127, 2008.
26. Tuli, R., Nandi, S., Li, W.J., Tuli, S., Huang, X., Manner, P.A., Laquerriere, P., Noth, U., Hall, D.J., and Tuan, R.S. Human mesenchymal progenitor cell-based tissue engineering of a single-unit osteochondral construct. Tissue Eng **10,** 1169, 2004.
27. Landers, R., Hubner, U., Schmelzeisen, R., and Mulhaupt, R. Rapid prototyping of scaffolds derived from thermoreversible hydrogels and tailored for applications in tissue engineering. Biomaterials **23,** 4437, 2002.
28. Meyvis, T.K., Stubbe, B.G., Van Steenbergen, M.J., Hennink, W.E., De Smedt, S.C., and Demeester, J. A comparison between the use of dynamic mechanical analysis and oscillatory shear rheometry for the characterisation of hydrogels. Int J Pharm **244,** 163, 2002.
29. Siddappa, R., Martens, A., Doorn, J., Leusink, A., Olivo, C., Licht, R., van Rijn, L., Gaspar, C., Fodde, R., Janssen, F., van Blitterswijk, C., and de Boer, J. cAMP/PKA pathway activation in human mesenchymal stem cells *in vitro* results in robust bone formation *in vivo*. Proc Natl Acad Sci U S A **105,** 7281, 2008.
30. Masuda, K., Sah, R.L., Hejna, M.J., and Thonar, E.J. A novel two-step method for the formation of tissue-engineered cartilage by mature bovine chondrocytes, the alginate-recovered-chondrocyte (ARC) method. J Orthop Res **21,** 139, 2003.
31. Guo, J.F., Jourdian, G.W., and MacCallum, D.K. Culture and growth characteristics of chondrocytes encapsulated in alginate beads. Connect Tissue Res **19,** 277, 1989.
32. Moroni, L., de Wijn, J.R., and van Blitterswijk, C.A. Integrating novel technologies to fabricate smart scaffolds. J Biomater Sci Polym Ed **19,** 543, 2008.
33. Cohen, D.L., Malone, E., Lipson, H., and Bonassar, L.J. Direct freeform fabrication of seeded hydrogels in arbitrary geometries. Tissue Eng **12,** 1325, 2006.
34. Lee, W., Debasitis, J.C., Lee, V.K., Lee, J.H., Fischer, K., Edminster, K., Park, J.K., and Yoo, S.S. Multi-layered culture of human skin fibroblasts and keratinocytes through three-dimensional freeform fabrication. Biomaterials **30,** 1587, 2009.
35. Song, F., Zhang, L.M., Li, N.N., Shi, J.F. *In situ* crosslinkable hydrogel formed from a polysaccharide-based hydrogelator. Biomacromolecules **10,** 959, 2009.
36. Haines-Butterick, L., Rajagopal, K., Branco, M., Salick, D., Rughani, R., Pilarz, M., Lamm, M.S., Pochan, D.J., and Schneider, J.P. Controlling hydrogelation kinetics by peptide design for three-dimensional encapsulation and injectable delivery of cells. Proc Natl Acad Sci U S A **104,** 7791, 2007.
37. Engler, A.J., Sen, S., Sweeney, H.L., and Discher, D.E. Matrix elasticity directs stem cell lineage specification. Cell **126,** 677, 2006.
38. Fedorovich, N.E., Alblas, J., de Wijn, J.R., Hennink, W.E., Verbout, A.J., and Dhert, W.J. Hydrogels as extracellular matrices for skeletal tissue engineering: state-of-the-art and novel application in organ printing. Tissue Eng **13,** 1905, 2007.
39. Koike, N., Fukumura, D., Gralla, O., Au, P., Schechner, J.S., and Jain, R.K. Tissue engineering: creation of long-lasting blood vessels. Nature **428,** 138, 2004.
40. Mironov, V., Reis, N., and Derby, B. Review: bioprinting: a beginning. Tissue Eng **12,** 631, 2006.
41. Grayson, W.L., Bhumiratana, S., Grace Chao, P.H., Hung, C.T., and Vunjak-Novakovic, G. Spatial regulation of human mesenchymal stem cell differentiation in engineered osteochondral constructs: effects of pre-differentiation, soluble factors and medium perfusion. Osteoarthritis Cartilage **18,** 714, 2010.

42. Schuurman, W., Khristov, V., Pot, M.W., van Weeren, P.R., Dhert, W.J., and Malda, J. Bioprinting of hybrid tissue constructs with tailorable mechanical properties. Biofabrication **3,** 021001, 2011.
43. Kim, T.K., Sharma, B., Williams, C.G., Ruffner, M.A., Malik, A., McFarland, E.G., and Elisseeff, J.H. Experimental model for cartilage tissue engineering to regenerate the zonal organization of articular cartilage. Osteoarthritis Cartilage **11,** 653, 2003.
44. Mironov, V., Boland, T., Trusk, T., Forgacs, G., and Markwald, R.R. Organ printing: computer-aided jet-based 3D tissue engineering. Trends Biotechnol **21,** 157, 2003.
45. Lee, M.G., Choi, S., and Park, J.K. Three-dimensional hydrodynamic focusing with a single sheath flow in a single-layer microfluidic device. Lab Chip **9,** 3155, 2009.
46. Elloumi Hannachi, I., Itoga, K., Kumashiro, Y., Kobayashi, J., Yamato, M., and Okano, T. Fabrication of transferable micropatterned-co-cultured cell sheets with microcontact printing. Biomaterials **30,** 5427, 2009.
47. Williams, D.F. On the mechanisms of biocompatibility. Biomaterials **29,** 2941, 2008.
48. Thonhoff, J.R., Lou, D.I., Jordan, P.M., Zhao, X., Wu, P. Compatibility of human fetal neural stem cells with hydrogel biomaterials *in vitro*. Brain Res **1187,** 42, 2008.
49. Khattak, S.F., Bhatia, S.R., and Roberts, S.C. Pluronic F127 as a cell encapsulation material: utilization of membrane-stabilizing agents. Tissue Eng **11,** 974, 2005.
50. Vermonden, T., Fedorovich, N.E., van Geemen, D., Alblas, J., van Nostrum, C.F., Dhert, W.J., and Hennink, W.E. Photopolymerized thermosensitive hydrogels: synthesis, degradation, and cytocompatibility. Biomacromolecules **9,** 919, 2008.
51. Fedorovich, N.E., Swennen, I., Girones, J., Moroni, L., van Blitterswijk, C.A., Schacht, E., Alblas, J., and Dhert, W.J. Evaluation of photocrosslinked lutrol hydrogel for tissue printing applications. Biomacromolecules **10,** 1689, 2009.
52. Schagemann, J.C., Chung, H.W., Mrosek, E.H., Stone, J.J., Fitzsimmons, J.S., O'Driscoll, S.W., and Reinholz, G.G. Poly-epsilon-caprolactone/gel hybrid scaffolds for cartilage tissue engineering. J Biomed Mater Res A **93,** 454, 2010.
53. Endres, M., Hutmacher, D.W., Salgado, A.J., Kaps, C., Ringe, J., Reis, R.L., Sittinger, M., Brandwood, A., and Schantz, J.T. Osteogenic induction of human bone marrow-derived mesenchymal progenitor cells in novel synthetic polymer-hydrogel matrices. Tissue Eng **9,** 689, 2003.

Address correspondence to:
Jacqueline Alblas, Ph.D.
Department of Orthopaedics G05.228
University Medical Center Utrecht
P.O. Box 85500
3508 GA Utrecht
The Netherlands

E-mail: j.alblas@umcutrecht.nl

Received: February 01, 2011
Accepted: August 19, 2011
Online Publication Date: September 28, 2011